1 **Exploring the sensitivity on a soil area-slope-grading relationship**

2 **to changes in process parameters using a pedogenesis model**

7 W.D. D.P. Welivitiya[1,2], Garry R Willgoose[1], Greg R Hancock[2], and [3]Sagy Cohen

9 [1]School of Engineering, The University of Newcastle, Callaghan, 2308, Australia

10 [2]School of Environment and Life Sciences, The University of Newcastle, Callaghan, 2308,
11 Australia

12 [3]Department of Geography, University of Alabama, Box 870322, Tuscaloosa, Alabama
13 35487, USA

15 Corresponding Author: Garry Willgoose

16   Garry.willgoose@newcastle.edu.au

18 Submitted to: Earth System Dynamics (ESD)

1 **Abstract**

2   This paper generalises the physical dependence of the relationship between

3 contributing area, local slope, and the surface soil grading first described by *Cohen et al*,

4 [2009, 2010] using their mARM1D and mARM3D pedogenesis models. A more general

5 computational model, SSSPAM5D, extending the conceptualisation of mARM3D has been

6 developed to further our exploration of soilscape self-organisation. A parametric study was

7 carried out using different parent materials, erosion, and weathering mechanisms. These

8 simulations confirmed the generality of the area-slope-d_{50} relationship. The relationship is

9 also true for other statistics of soil grading (e.g. d_{10}, d_{90}) and robust for different depths within

10 the profile. For small area-slope regimes (i.e. hillslopes with small areas and/or slopes) only

11 the smallest particles can be mobilised by erosion and the area-slope-d_{50} relationship appears

12 to reflect the erosion model and its Shields Stress threshold. For higher area-slope regimes,

13 total mobilization of the entire soil grading occurs and self-organisation reflects the relative

14 entrainment of different size fractions. Occasionally the interaction between the in-profile

15 weathering and surface erosion draws the bedrock to the surface and forms a bedrock

16 outcrop. The study also shows the influence on different depth dependent in-profile

17 weathering functions in the formation of the equilibrium soil profile and the grading

18 characteristics of the soil within the profile.

1. Introduction

The importance of soil in environmental processes is well established [*Jenny*, 1941; *Bryan*, 2000; *Strahler and Strahler*, 2006; *Lin*, 2011]. However spatially distributed quantification of soil properties is difficult because of the complexity and dynamic nature of the soil system itself [*Hillel*, 1982]. The necessity for quantified and spatially distributed soil functional properties is clear [*Behrens and Scholten,* [2006]; *McBratney et al.,* [2003]]. Moreover, explicit soil representation in models of environmental processes and systems (e.g. landform evolution, and hydrology models) has increased rapidly in the last few decades. For optimum performance these physically-based and spatially-explicit models demand high quality spatially distributed soil attributes [*McBratney et al.*, 2003].

The need for improved soil data arises in two main areas: (1) better mapping of the description of the soil (e.g. grading, soils classification), and (2) improved representation of soil functional properties (e.g. hydraulic conductivity, water holding capacity). For most environmental models it is the soil functional properties that are of greatest interest since they determine the pathways and rates of environmental process. Accordingly this paper is focussed on a soil representation that can underpin the derivation of functional properties. Pedotransfer functions exist (albeit with large uncertainty bounds) to then relate these soil descriptions to functional properties. The existence of these pedotransfer functions intellectually underpins the rationale of the work in this paper. While these techniques are not the focus of this paper, some discussion of them is pertinent so that the importance of the scaling relationship discussed in this paper can be fully appreciated.

Traditional soil mapping typically used field sampling and classified soils into different categories based on a mixture of quantitative (e.g. pH) and qualitative features (e.g. colour). They do not directly provide the functional soil properties required by environmental models. Several techniques have been introduced to tackle this lack of functional description such as pedotransfer functions, geostatistical approaches, and state-factor (Clorpt) approaches [*Behrens and Scholten*, 2006]. Pedotransfer functions (PTFs) have been developed to predict functional soil properties using easily measurable soil properties such as particle size grading, organic content, and clay content. However useful these PTFs are, they are limited because they need spatially distributed soil descriptions and, in many cases, site specific calibration [*Benites et al.*, 2007]. Geostatistical approaches interpolate field data to create soil-attribute maps. Clorpt or Scorpan approaches [*McBratney et al.*, 2003] use regression or fuzzy-set theory to create soil-attribute or soil-class maps [*Behrens and Scholten*, 2006].

1   Geostatistical digital soil mapping using field sampling of soil is possible for a

2   specific site where the area is small [*Scull et al.*, 2003]. However, it can be prohibitively

3   expensive and time consuming for larger sites. Soil mapping techniques, such as Clorpt or

4   Scorpan, use digitization of existing soil maps. They generate soil classes through decision

5   tree methods and artificial neural networks using easily measurable soil attributes (similar to

6   PTFs) and have been used to generate digital soil maps [*McBratney et al.*, 2003]. Although

7   much work has been carried out they also suffer the need for site-specific calibration.

8   Remote sensing technologies such as gamma ray spectroscopy have introduced novel

9   methods of characterizing soil properties and developing digital soil maps. However at the

10   present state of technology, these gamma ray spectral imaging devices are used as hand held

11   devices or airborne survey instruments. For this reason, although the spatial resolution of

12   digital soil maps produced by gamma ray spectroscopy is relatively coarse and their spatial

13   coverage is limited their links with functional properties remain uncertain [*McBratney et al.*,

14   2003].

15   Developments in geographic information systems (GIS) have enabled fast and

16   efficient characterization and analysis of large amounts of spatial and non-spatial data [*Scull*

17   *et al.*, 2003]. Products of GIS technology such as digital elevation models (DEM) have

18   revolutionized the study of geomorphological processes through physically based numerical

19   modelling [*Singh and Woolhiser*, 2002]. This is the rationale for the GlobalSoilMap

20   initiative, which aims to provide a global 90m map of soil properties for the world (Sanchez

21   et al., 2009). Methodologies to predict the soil characteristics using morphological attributes

22   and models of physical processes derived from digital elevation models (e.g. contributing

23   area, slope) were developed by *Sharmeen and Willgoose* [2006] using their physically based

24   model ARMOUR. ARMOUR used overland flow driven armouring, and weathering to drive

25   the evolution of soil on a hillslope. However, the very high computing resources and long run

26   times of the physically based modelling prevented them from coupling ARMOUR with a

27   hillslope evolution model.

28   *Cohen et al.* [2009] developed a state-space matrix soils model, mARM1D, and

29   calibrated it to output from ARMOUR. mARM1D was significantly more computationally

30   efficient than ARMOUR, and was able to simulate more complex hillslope geometries. It was

31   sufficiently fast that it could be used to simulate the spatial distribution of the soil profile as

32   well the surface properties. By incorporating the weathering characteristics of soil profile into

1   mARM1D, *Cohen et al.* [2010] developed mARM3D which was able to explore the

2   evolution of soil profile at small catchment scale. *Cohen et al.* [2009] using pedogenic

3   processes was the first to identify using pedogenic processes a relationship between the

4   hillslope soil grading, and the hillslope gradient. However, it was only tested for a small

5   number of cases, and for one set of climate and pedogenic data.

6   Clearly there is a need to test the robustness and generality of the area-slope-grading

7   relationship for a broader range of conditions. This paper generalises the mARM3D

8   formulation and extends its numerics to allow us to test the relationship for more general

9   conditions. We present the results and insights obtaining by the new modelling framework,

10   State Space Soilscape Production and Assessment Model (SSSPAM). The state-space based

11   model we developed using the SSSPAM framework simulates soil evolution in 5 dimensions.

12   They are the 2 horizontal dimensions (i.e. x and y), depth down the soil profile, time, and the

13   soil grading with depth: thus the suffix 5D.

14   1.1   Armouring

15   The first important process is armouring as a result of fluvial erosion. Armouring in

16   river beds has been widely understood and studied extensively for mostly streams and rivers

17   [*Gessler*, 1970; *Gomez*, 1983; *Lisle and Madej*, 1992; *Little and Mayer*, 1976; *Parker and*

18   *Klingeman*, 1982]. The majority of these armouring models employ time varying simulations

19   to calculate the particle distribution of the armour layer by selective entrainment of the

20   smaller bed material by the transport medium.

21   Armouring of the surface soil layer is a by-product of erosion by either overland water

22   flow (fluvial erosion) or wind (aeolian erosion). Depending on the energy of the erosion

23   medium, transportable fine particles are preferentially entrained and transported from the

24   surface soil layer. This process coarsens the remaining surface soil layer enriching it with

25   coarser, less mobile, material. With time, if the energy of the transport medium remains

26   constant, an armoured layer is formed with all the transportable material removed. At this

27   time the sediment transport reaches zero. This armour, where all the materials are larger than

28   the largest grains which the transport medium can entrain, prevents erosion of material from

29   the subsurface. If the energy of the transport medium increases, the existing armour can be

30   disrupted, and a newer stable armour with coarser material can be formed [*Sharmeen and*

31   *Willgoose*, 2006].

1.2 Weathering

The second important process is weathering. Weathering is a general term used to describe all the processes which cause rocks or rock fragments to disintegrate or alter through physical, chemical or biological means [*Strahler and Strahler*, 2006]. Disintegration of rock material through physical weathering can occur by (1) unloading, (2) expansion and contraction of rock through heating and cooling cycles, (3) stress developing in rock fractures due to freezing water, (4) salt crystal growth or tree root intrusions, and (4) abrasion of rock by harder materials transported by flowing water or glaciers [*Thornbury*, 1969]. Physical weathering where larger soil particles are broken down into smaller particles is dominant in the surface layer of material where it is more exposed. Weathering also occurs underneath the surface and the weathering rate at these subsurface layers can be modelled with depth dependent weathering functions.

There is considerable literature concentrating on different aspects of rock weathering such as physical weathering [*Ollier*, 1984; *Wells et al.*, 2006; *Wells et al.*, 2008; *Yokoyama and Matsukura*, 2006] and chemical weathering [*Green et al.*, 2006; *Ollier*, 1984]. However the significance of the combination of armouring and weathering, and the influence on soil erosion in landform evolution models has only recently been quantitatively studied [*Sharmeen and Willgoose*, 2006].

1.3 Modelling approaches

The combined effect of armouring and weathering on the soil evolution on hillslopes was first explored by *Sharmeen and Willgoose* [2006]. They investigated interactions between particle weathering and surface armouring and its effect on erosion using a physically based one dimensional hillslope soil erosion model called ARMOUR. To carry out their simulations they used surface soil grading data from two mine sites (1) Ranger Uranium Mine (Northern Territory, Australia), and (2) Northparkes Gold Mine (New South Wales, Australia). They demonstrated that the influence of weathering was significant in the armouring process, sediment flux, and erosion rate. Using ARMOUR they demonstrated the feasibility of using a physically based model to represent soil evolution in studying geomorphological evolution and as a simple model for pedogenesis. The main drawback of the numerical approximation used in ARMOUR model was it's high computational complexity and very long run times which prevented it from being used for more complex

1   geometries such as 2D catchments [*Cohen et al.*, 2009], or its coupling with a landform

2   evolution mdoel.

3   A significant advance occurred when *Cohen et al.* [2009] simplified ARMOUR by

4   reformulating it as a state-space matrix model, mARM1D, where the complex nonlinear

5   physical processes in ARMOUR were modelled using transition matrices. By doing so Cohen

6   was able to reduce the numerical complexity of ARMOUR and significantly reduce runtimes.

7   The computational efficiency of mARM1D allowed Cohen to explore (1) time-and space-

8   varying relationships between erosion and physical weathering rates at the hillslope scale, (2)

9   more complex planar drainage geometries, and (3) interactions between the soil profile and

10   the soil surface properties. They found that for erosion-dominated slopes the surface coarsens

11   over time, while for weathering dominated slopes the surface fines over time. When both

12   processes operate simultaneously a slope can be weathering-dominated upslope (where runoff

13   and therefore erosion is low) and armouring-dominated downslope. In all cases, for a

14   constant gradient slope the armour coarsens downslope (i.e. as drainage area increases) as a

15   result of a balance between erosion and weathering. Thus even for weathering-dominated

16   slopes the surface grading catena is dependent on armouring through the balance between

17   weathering and armouring [*Cohen et al.*, 2009]. They also observed that for many slopes the

18   surface initially armours but, after some period of time (space and rate dependent),

19   weathering begins to dominate and the surface subsequently fines. Depending on the relative

20   magnitude of armouring and weathering the final equilibrium grading of the slope may be

21   finer or coarser than the initial conditions but in all cases the surface coarsened with

22   increasing area and slope. These results were in good agreement with the results of the

23   ARMOUR model used by *Sharmeen and Willgoose* [2006]. The work of both Sharmeen and

24   Cohen used process parameters calibrated to field erosion [*Willgoose and Riley*, 1998] and

25   laboratory weathering data [*Wells et al.*, 2006; *Wells et al.*, 2008] for a site at Ranger

26   Uranium Mine. Thus their conclusions only apply to the site at Ranger.

27   The aim of this paper is to present a new model (SSSPAM5D) that extends this

28   previous work and allows more general assessments and predictions of pedogenesis. Here we

29   present (1) the extensions in SSSPAM5D, (2) calibration and validation of SSSPAM5D, and

30   (3) exploration of the spatial and temporal patterns of soil grading and weathering and

31   armouring processes. The model discussed here is the soilscape component of a coupled soil-

1 landscape evolution model and this paper aims to better understand the behaviour of this

2 soilscape model before examining the more complex coupled system.

4 **2. The SSSPAM5D model**

5   SSSPAM5D is a state-space matrix model simulating temporal and spatial variation

6 of the grading of the soil profile through depth over a landscape and extends the approach of

7 the mARM1D model (*Cohen et al.,* 2009) and mARM3D (*Cohen et al.* 2010). It uses matrix

8 equations to represent physical processes acting upon the soil grading through the soil profile.

9 SSSPAM5D uses the interaction between a number of layers to simulate soil grading

10 evolution (Figure 1). These layers are: (1) A water layer flowing over the ground which

11 moves soil particles laterally, (2) a surface soil layer from which the water entrains soil

12 particles and which produces an armour over the soil below, (3) several soil layers

13 representing the soil profile, and (4) a semi-infinite non-weathering bedrock/saprolite layer

14 underlying the soil.

15   The soil grading at any specific time, and for any specific layer, is given by a vector,

16 the state vector. Each entry in the state vector is the mass of sediment in each grading size

17 range in that layer. The transition from the state at any given time to the state at the next time

18 step (i.e. the change in soil grading from one timestep to the next) is described by a matrix

19 equation. Two processes are modelled: erosion due to overland flow, and weathering within

20 the profile. The armouring module consists with 3 principle components.

21   The grading of the surface (armour) layer changes over time because of three

22 competing processes, (1) selective entrainment of finer fractions by erosion, (2) the resupply

23 of material from the subsurface (that balances the erosion to ensure mass conservation in the

24 armour layer) and (3) the breakdown of the particles within the armour due to physical

25 weathering. The erosion rate of the armour layer is calculated from the flow shear stress. The

26 entrainment of particles into surface flow at each time step from the armour layer is

27 determined by the erosion transition matrix, which is constructed using Shield shear stress

28 threshold. The Shield shear stress threshold determines the maximum particle size that can be

29 entrained in the surface water flow. For particles smaller than the Shield's shear stress

30 threshold a selective entrainment mechanism is used which was found to be a good fit to field

31 data [*Willgoose and Sharmeen*, 2006]. Resupply of particles to the armour layer from below

1   is mass conservative. The rate of resupply equals the rate of erosion, so the armour's mass is

2   constant.

3   The weathering module simulates the disintegration of particles in the armour and

4   underlying soil profile layers. Weathering is also modelled with a transition matrix. It defines

5   the change in the armour grading as a result of the fracturing of particles through the

6   weathering mechanism. The "Body Fracture" mechanism (Figure 2) splits the parent particle

7   into a number of daughter particles. *Wells et al.* [2008] found that a body fracture model with

8   2 equal-volume daughter fragments best fitted his laboratory salt weathering experiments.

9   This does not guarantee that this fragmentation mechanism is appropriate for other rock types

10   not tested by Wells, and one of the cases studied in this paper is a generalisation of this equal

11   volume fragmentation geometry. Weathering in this paper is mass conservative so that when

12   larger particles break into smaller particles and the cumulative mass of the soil grading

13   remains constant.

14   The soil grading at a specific time and layer is defined by the state vector $\underline{g}$. Entries

15   g_i in the state vector $\underline{g}$ are proportion of the material in the grading size range i. The

16   evolution (of the state vector) from one state to another state during a single time step is

17   defined using a matrix equation. This matrix (called the transition matrix) describes the

18   relationship between the states at two times and defines the change in the state during a time

19   step

$$\underline{g}_{t_2} = \left(\mathbf{I} + \mathbf{R}\Delta t\right)\underline{g}_{t_1} \qquad (1)$$

21   where $\underline{g}_{t_1}$ and $\underline{g}_{t_2}$ are state vectors defining the soil grading at time t_1 and t_2, $\mathbf{R}$ is the

22   marginal transition matrix, $\mathbf{I}$ is the identity matrix, and Δt is the timestep [*Cohen et al.*,

23   2009].

24   For multiple processes Equation (1) can be applied sequentially for each process, using the $\mathbf{R}$

25   matrix appropriate for each of the processes.

26   Within each layer the equation for weathering follows equation (1)

$$\underline{g}_{t_2} = \left[\mathbf{I} + \left(W\Delta t\right)\mathbf{B}\right]\underline{g}_{t_1} \qquad (2)$$

1 where W is the rate of weathering (which is depth dependent), and **B** is the non-dimensional

2 weathering marginal transition matrix. Parameter W determines the rate of weathering while

3 **B** determines the grading characteristics of the weathered particles.

4   For the armour layer the mass in the layer is kept constant so that as fines are

5 preferentially removed by erosion, the mass removed is balanced by new material added from

6 the layer below, and with the grading of the layer below. For each layer in the profile mass

7 conservation is applied, and any net deficit in mass is (typically) made up from the layer

8 below (i.e. by removing material in the layer below). The only exception to this rule is the

9 case of deposition at the surface where material is pushed down. In this latter case the

10 pushing down results from an excess of mass in the armour layer and this excess propagates

11 down through the profile.

12 **2.1. Constitutive Relationships for Erosion and Armouring**

14   The erosion rate (E) of the armour is calculated by,

$$E = e \frac{q^{\alpha_1} S^{\alpha_2}}{d_{50_a}^{\beta}} \qquad (3)$$

16 Where e is the erodibility rate, q is discharge per unit width (m^3/s/m), S is slope, d_{50_a} is the

17 median diameter of the material in the armour (m), α_1, α_2 and β are exponents governing

18 the erosion process. It is possible to derive exponents α_1 and α_2 from the shear stress

19 dependent erosion physics [*Willgoose et al.*, 1991b] or they can be calibrated to field data

20 (e.g. *Willgoose and Riley* [1998]). In this paper for simplicity we will consider a two-

21 dimensional hillslope with a unit width, constant gradient, and a 2m maximum soil depth.

22 The discharge was calculated by

$$q = rx \qquad (4)$$

26   The implementation details of the erosion physics (e.g. how selective entrainment of

27 fines is incorporated into the marginal transition matrix for erosion) are identical to that of

28 Cohen et al., (2009) and will not be discussed here. The primary process of relevance here is

29 that a size selective entrainment of fine fractions of the soil grading by erosion is used and it

1   follows the approach of Parker and Klingeman (1982) as calibrated by Willgoose and

2   Sharmeen (2006). The result is that for surfaces that are being eroded the surface becomes

3   coarser with time (and thus why we call the top layer the armour layer).

4   **2.2 Constitutive Relationships for Weathering**

5   The fracturing geometry determines the weathering transition matrix **B**. Each grading

6   size class will lose some of its mass to smaller grading size classes as larger parent particles

7   are transformed into smaller daughter particles. The daughter products can fall in one or more

8   smaller grading classes depending on the size range of particles produced by the breakdown

9   of the larger parent particles. The amount of material received by each smaller size class is a

10 function of size distribution of the grading classes, fracture mechanism and the size

11 characteristics of the daughter particles.

12   *Wells et al.* [2008] found that for his material (a mining waste product from Ranger

13 Uranium Mine) a simple symmetric fracture model with two equal volume daughter products

14 best fitted his experimental data. While the formulation of the weathering transition matrix in

15 Cohen et al., (2009) allows a general fragmentation geometry, Cohen only used the

16 symmetric fragmentation found experimentally by Wells. This paper will generalise these

17 results and examine a broader range of fracture geometries.

18   To generalise the fracture geometries we will assume that a parent particle with a

19 diameter d breaks into a single daughter particle with diameter d_1 and $n-1$ smaller

20 daughters with diameter d_2 (the total number of daughters being n). For simplicity all the

21 particles considered are assumed to be spherical. Mass conservation implies

$$d^3 = d_1^3 + (n-1)d_2^3 \qquad (5)$$

23 If the single larger daughter with diameter d_1 accounts for α fraction of the parent then

$$d_1 = \alpha^{\frac{1}{3}} d \qquad (6)$$

$$d_2 = \left(\frac{1-\alpha}{n-1}\right)^{\frac{1}{3}} d \qquad (7)$$

1   By changing the α fraction value and the number of daughters n we are able to simulate

2   various fracture geometries such as symmetric fragmentation, asymmetric fragmentation, and

3   granular disintegration [*Wells et al.*, 2008]. For instance α =0.5, n =2 represents symmetric

4   fragmentation with 2 daughter particles, α =0.99 , n=11 represents a fracture mechanism

5   resembling granular disintegration where a large daughter retains 99% of the parent particle

6   volume and 10 smaller daughters have 1% of the parent volume collectively.

7   The construction of the weathering transition matrix then follows the methodology

8   outlined in Figure 1 in Cohen et al., (2009).

9   **2.3 Soil profile development through depth dependent weathering**

10   The weathering module of SSSPAM5D consists of 2 components. They are (1) the

11   weathering geometry for the grading of the daughter particles, and (2) the weathering rate for

12   the different soil layers which determines the rate at which the parent material is weathered.

13   The weathering rate of each soil layer typically (though not always) depends on the depth

14   below the soil surface.

15   To characterize the weathering rate with soil depth, depth-dependent weathering

16   functions are used. In their mARM3D model Cohen et al. [2010] used 2 depth-dependent

17   weathering functions (Figure 3), (1) exponential decline (called exponential) [Humphreys and

18   Wilkinson, 2007] and (2) humped exponential decline (called humped) [Ahnert, 1977;

19   Minasny and McBratney, 2006]. In the exponential, the weathering rate declines

20   exponentially with depth. The rationale underpinning this function is that the surface soil

21   layer is subjected to the high rates of weathering because it is closer the surface where

22   wetting and drying, and temperature fluctuations are greatest. The humped function has the

23   maximum weathering rate at a finite depth below the surface instead of being at the surface

24   itself and then declines exponentially below that depth. For example, there is evidence that

25   the weathering is highest at the water table surface which leads to a humped function.

26   In addition to these functions we used another depth dependent weathering function

27   we call the dynamic reversed exponential function (called hereafter reversed exponential). In

28   this function the highest weathering rate is located at the soil-bedrock interface and

29   exponentially decreases upwards toward the surface and downwards into the underlying

30   bedrock. Unlike the exponential and humped functions the depth of the peak weathering rate

31   in the dynamic reversed exponential function moves up and down with the ups and downs of

1 the soil-bedrock interface. At the soil-bedrock interface the bedrock material is transformed

2 from bedrock to soil. The bedrock has a higher potential for chemical weathering than the soil

3 above the soil-bedrock interface that has been subjected to chemical weathering. The function

4 decline below the soil-bedrock interface because of the reduced porosity of the bedrock

5 inhibits water flow. Although we do not explicitly model chemical weathering in this paper,

6 we believe that the dynamic reversed exponential function can be used to conceptualise

7 chemical weathering.

8   The three depth dependent weathering functions are graphically represented by Figure

9 3. The exponential function is (*Cohen et al.*, 2010)

$$w_h = \beta' e^{(-\delta_1 h)} \tag{8}$$

11 where w_h is the weathering rate at the soil layer at a depth of h (m) below the surface and δ_1

12 is the depth scaling factor (here $\delta_1 = 1.738$)

13   The humped function used is (*Minasny and McBratney*, 2006)

$$w_h = \frac{P_0 \left[e^{(-\delta_2 h + P_a)} - e^{(-\delta_3 h)} \right]}{M} \tag{9}$$

16 where P_0 and P_a are the maximum weathering rate and the steady state weathering rate

17 respectively, δ_2 and δ_3 are constants used to characterise the shape of the function, and M is

18 the maximum weathering rate at the hump which is used to normalize the function. Values

19 we used here were $P_0 = 0.25$, $P_a = 0.02$, $\delta_2 = 4$, $\delta_3 = 6$, and $M = 0.04$.

20   The dynamic reversed exponential function is

$$w_h = \begin{cases} 1 - \lambda \left[1 - e^{-\delta_4 (H-h)} \right] & \text{for} \quad h \leq H \\ 1 - \lambda \left[1 - e^{-\delta_5 (h-H)} \right] & \text{for} \quad h > H \end{cases} \tag{10}$$

1   where H is the depth to the soil bedrock interface from the surface (m) which is calculated

2   from the soil grading distribution at each iteration during the simulation, λ is a constant which

3   determines the function value at the asymptote, δ_4 and δ_5 are constants used to characterise

4   the rate of decline with depth of the function. We used $\lambda = 0.98$, $\delta_4 = 3$, $\delta_5 = 10$.

5   The non-zero weathering below the bedrock-soil interface represents a slower rate of

6   chemical weathering within the bedrock due to its lower porosity and hydraulic conductivity.

7   In general $\delta_5 > \delta_4$.

8   The weathering rate of each layer is determined by modifying the base weathering

9   rate W_0 (Equation 2) and the depth dependent weathering function used, $f(h)$. The

10   weathering rate of a soil layer at a depth of h from surface W_h is given by,

$$W_h = W_0 f(h) \qquad (11)$$

12   **3. Data used in this study**

13   Four soil particle size distribution data sets were used as input data for SSSPAM5D

14   simulations. Two particle size distribution data sets were collected from the Ranger Uranium

15   Mine (Northern Territory, Australia) spoil site [*Cohen et al.*, 2009; *Coulthard et al.*, 2012;

16   *Sharmeen and Willgoose*, 2007; *Willgoose and Riley*, 1998]. The third and fourth gradings

17   were created from the previous two gradings to simulate the subsurface bedrock conditions

18   (Table 1).

19   • Ranger1a: This grading distribution was first used by *Willgoose and Riley* [1998] for

20   their landform evolution modelling experiments. This soil grading was subsequently

21   used by *Sharmeen and Willgoose* [2007] and *Cohen et al.* [2009] for their armouring

22   and weathering simulations. This grading distribution consists of stony metamorphic

23   rocks of medium to coarse size produced by mechanical weathering breakdown, has a

24   median diameter about 3.5mm, and has a maximum diameter of 19mm.

25   • Ranger2a: The second grading distribution was used by *Coulthard et al.* [2012] in

26   their soil erosion modelling experiments and has a maximum diameter of 200mm.

27   The Coulthard set includes a coarse fraction not included in Ranger 1a, has a median

28   diameter of 40mm, and has a maximum diameter of 200mm. Nominally Gradings 1a

29   and 2a are for the same site but the gradings are not identical in the overlapping part

30   of the grading below 19mm.

1   •   Ranger1b and Ranger2b: These grading data sets were created using the particle

2   distribution classes of Ranger1a and Ranger2a to represent the underlying bedrock for

3   each of the grading distributions mentioned above. To represent the bedrock for these

4   data sets 100% of the material was assumed to be in the largest diameter class for

5   each grading classes (19mm for the 1b and 200mm for 2b).

7   We divided our planar hillslope into nodes with 4m spacing downslope and the

8   armouring and weathering was simulated at these nodes. We have used 30 years of measured

9   pluviograph data [*Willgoose and Riley*, 1998] to calculate discharge. The 30 years of runoff

10   was repeated to create a 100-year data set as was done in our earlier work (*Sharmeen and*

11   *Willgoose* [2006]; *Cohen et al.* [2009]).

13   **4. SSSPAM5D calibration**

14   To provide a starting point for the parametric study SSSPAM5D was calibrated to

15   mARM3D, which in turn had been calibrated to ARMOUR1D (Willgoose and Sharmeen,

16   2006) and which had been compared with field data. The parametric study then varied the

17   parameters around these values.

18   Figure 4 shows a comparison between contour plots generated by mARM3D and

19   SSSPAM5D using identical initial conditions (Ranger grading data set 1) and model

20   parameters. The figure shows that mARM3D and SSSPAM5D produce similar d_{50} values.

21   The minor differences between the two contour plots result from different plotting packages

22   (SURFER for mARM1D, matplotlib for SSSPAM5D). We are thus confident that

23   SSSPAM5D and mARM3D are comparable. The parameter values used for SSSPAM5D are

24   $\alpha_1 = 1.0$, $\alpha_2 = 1.2$, $\beta = 1.0$, $m = 4$, $e = 2.5 \times 10^{-8}$ and $n = 0.1$.

1   **5. SSSPAM5D Simulations and results**

2   *Cohen et al.* [2009, 2010] found a strong log-log linear relationship between

3   contributing area, slope and the d_{50} of the armour soil grading. It quantifies the relationship

4   between soil grading, local topographic gradient and drainage area such that

$$\frac{A^{\alpha}S}{d_{50}{}^{\varepsilon}} = \text{constant} \qquad (12)$$

7   where A is the contributing area to the point of interest, S is the slope of the point of interest,

8   d_{50} is the 50th percentile (i.e. median) of the soil grading, and α and ε are constants. Here

9   we will examine other statistics of the profile soil grading. Cohen used only one parent

10   material grading and one parameter set for his analyses. To explore the generality of this

11   area-slope-grading relationship, in this section we examined the behaviour of the contour

12   plots with changes to (1) weathering parameters, (2) grading of the parent material, (3)

13   process and climate parameters, and (4) armouring mechanisms. We also examined a broader

14   range of area-slope combinations that would typically occur in nature. For the initial

15   conditions, unless otherwise indicated, in each simulation the 'a' grading was used for the

16   initial surface layer and the corresponding 'b' bedrock grading for all the initial subsurface

17   layers (e.g. Ranger1a for the surface and Ranger1b for the subsurface). To ensure that the

18   hillslopes had reached equilibrium, the model simulated 100,000 years with grading data

19   output every 200 years. Equilibrium was assessed to occur when the grading of all nodes on

20   the hillslope stopped changing, typically well before 100,000 years.

21   **5.1. Interpretation of the grading contour plots**

22   Before discussing the parametric study and its myriad of contour plots, Figure 4 shows how

23   the contour plots can be used to estimate soil properties for any hillslope type. Five profiles

24   are illustrated:

25   1. This is a hillslope where the slope is increasing down the hillslope so is

26   concave down in profile and looks like a rounded hilltop. The d_{50} increases

27   down the hillslope (i.e. increasing area, moving from left to right in Figure 4).

28   All our contour plots increase from left to right and from bottom to top, so in

29   general concave hillslopes will always coarsen downslope.

2. This hillslope has constant slope downslope and, as similar to slope 1, will always coarsen downslope.

3. This hillslope has slopes that are decreasing downslope and is concave up. Importantly the gradient of the line in Figure 4 is less than the gradient of the contours so the hillslope coarsens downslope.

4. This hillslope is similar to 3 except that the rate of decrease of slope downstream is more severe so the gradient of the line in Figure 4 is steeper than the gradient of the contours. This hillslope fines downstream.

5. This hillslope is a classic catena profile with a rounded hilltop and a concave profile downstream of the hilltop. Tracking this hillslope downstream it will initially coarsen. As it transitions to concave up it will continue to coarsen until the rate of reduction of the hillslope slope is severe enough that is starts to fine downstream. Whether this latter region of fining occurs will depend on the concavity of the hillslope and whether it's strong enough relative to the gradient of the soil contours in Figure 4.

Thus it should be clear that the spatial distribution of soils, and any questions of downslope fining or coarsening of those soils, must depend on the interaction between the pedogenesis processes that produce the soils (and thus drive the area-slope dependence of soil grading) and landform evolution processes that generate those profiles (and the area-slope relations for those slopes). Ultimately deeper understanding of these links will only come from a coupled landscape-soilscape evolution model, but in this paper we confine ourselves to better understanding of the soilscape processes and the area-slope dependence of grading.

5.2. Parametric Study of SSSPAM5D

All the nominal parameters used in the parametric study are presented in Table 2. In order to fully explore the area-slope-d_{50} relationship a parametric study was carried out using SSSPAM5D. The area-slope-diameter relationship was derived by evolving the soil on a number of one-dimensional, constant width, planar hillslopes, each with a different slope, with evolution continuing until the soil reached equilibrium. A contour plot was then created where the soil grading metric (usually the median diameter, d_{50}) was contoured for a range of slopes and area. Because of the planar slope, only erosion occurs, no deposition. Erosion is a function of local discharge, slope and soil surface grading as indicated in Equation (3), and is assumed to be detachment limited. Detachment limitation means that the upstream sediment

1   loads do not impact on erosion rates. Hillslope elevations are not evolved (i.e. no landform

2   evolution occurs) which is equivalent to assuming that the soil evolves more rapidly than the

3   hillslope so that the soils equilibrate quickly to any landform changes.

5.2.1. Changing surface and subsurface gradings and weathering rate

7   Figure 5 shows the equilibrium contour plots generated for each grading data set with

8   different weathering rates. The equilibrium d_{50} decreases with increasing weathering rate.

9   Higher weathering rates more rapidly break down the larger particles. The equilibrium d_{50}

10   values remained the same if the initial surface grading was changed: e.g. using the Ranger1a

11   or Ranger2b grading data for the surface but with Ranger2b for the bedrock yielded identical

12   equilibrium d_{50} results. As weathering broke down the surface layer and it was eroded it was

13   replaced by the weathered bedrock material, which was identical when the same subsurface

14   grading and weathering mechanism was used. Finally a coarser subsurface grading led to a

15   coarser armour.

16   As in Cohen et al., (2010) the log-log linear area-slope-d_{50} relationship was observed

17   in all contour plots regardless of the weathering rate. Moreover the contour lines in the

18   contour plots all have the same slope. This implies that although the magnitude of the

19   coarseness of the equilibrium armour depends on the underlying soil grading and weathering

20   mechanism, the slope of the contours is independent of the subsurface grading and

21   weathering process. This result demonstrates that the area-slope-d_{50} relationship is robust

22   against changes in the grading of the source material.

5.2.2. Changing the Runoff Rate

25   The erosion process is a function of the discharge rate of water, and the discharge

26   depends on the climate and rainfall. The effect of changing the rainfall is shown in Figure 6.

27   To simulate a more arid climate the runoff generation parameter in Equation (4) was halved.

28   Figure 6 shows that a reduced discharge produced a finer armour. While not shown, higher

29   discharge rates produced a coarser armour. For lower discharges (1) the Shields Stress

30   threshold decreases thus allowing smaller particles to be retained in the armour layer, and (2)

31   the rate of erosion decreases while the weathering rate remains constant so that weathering

32   (i.e. fining) becomes more dominant. Both of these processes work in tandem to produce a

1 finer armour. This conclusion is consistent with Cohen et al., (2013), where they applied

2 natural climate variability over several ice-age cycles and observed switching between fining

3 and coarsening of the soil surface depending on the relative dominance of erosion and

4 weathering at that time in the climate cycle.

5 **5.2.3. Changing the erosion discharge and slope exponents**

6 The influence of the exponents on area and slope in the erosion equation (Equation 3),

7 α_1 and α_2, is shown in Figure 7. These contour plots used the Ranger site data set 1 for the

8 surface grading and Ranger bedrock grading for the initial subsurface layers. Figure 7 shows

9 that although the d_{50} values changed with different α_1 and α_2 values, the slope of the contours

10 only changed when α_1/α_2 was changed. To investigate the generality of this conclusion,

11 contours were then plotted for different α_1/α_2. The slope of the contours was strongly

12 correlated with α_1/α_2. The slope of the contours increased for higher α_1/α_2 ratios. Similar

13 results were obtained for the Ranger 2 data. The α_1/α_2 ratio not only influences the slope of

14 the contour lines but also influences the equilibrium d_{50} values. For low α_1/α_2, the equilibrium

15 d_{50} values at the hillslope nodes were coarser than for high α_1/α_2.

16 These relationships allow us to generalise the area-slope-d_{50} relationship

$$d_{50} = \left(cA^{\delta} S^{\gamma} \right)^{1/\varepsilon} \tag{13}$$

18 where δ, γ and ε are exponents on contributing area, slope and d_{50} respectively, and c is a

19 constant.

20 Table 3 and Figure 8 show that δ / γ was strongly correlated with the model α_1/α_2

21 even though there was no correlation with the individual parameters (i.e. α_1 with δ, or α_2

22 with γ). In the regression analysis the parameter ε was assumed to be 1 in order to calculate

23 δ and γ constants. This assumption does not affect the δ / γ ratio. This result was

24 independent of the subsurface grading.

25 **5.2.4. Changing the erosion exponent parameters β and e**

26 This section examines the effect of changing erosion equation parameters, (1) the

27 exponent β (Equation 3) which relates the erosion rate to median sediment diameter, and (2)

28 the erodibility rate e. The slope of the contours was independent of these parameters. The

29 parameters β and e influence (1) the absolute value of d_{50}, and (2) the spacing of the contours.

1 These impact on the value of c in Equation 13. For higher β, the equilibrium d_{50} was coarser

2 than for low β values. Increasing the erodibility factor e yields similar results.

5.2.5. Different weathering fragmentation geometries

4   To study different weathering mechanisms we used a fragmentation geometries that

5 has two parameters, n and α (Equations 5-7). The simulations in the previous sections used

6 symmetric fragmentation with $n=2$ and $\alpha=0.5$ (i.e. where a parent particle breaks down to

7 two equal volume daughter particles). Here we examine four other geometries, (1) symmetric

8 fragmentation with multiple daughter products ($n=5$, $\alpha=0.2$; i.e. the parent breaks into five

9 equal daughters each having 20% of the volume of the parent), (2) moderately asymmetric

10 ($n=2$, $\alpha=0.75$; the parent breaks into two daughters, with 75% and 25% of the parent volume),

11 (3) granular disintegration ($n=11$, $\alpha=0.9$; the parent breaks into 11 daughters, one with 90%

12 of the parent volume and the other 10 daughters each have 1% of the parent volume), and (4)

13 as for Geometry 3 but with the large daughter having 99% of the parent particle volume

14 ($n=11$, $\alpha=0.99$). Figure 9 shows results using the Ranger1 grading. The corresponding

15 symmetric results are in Figure 5. Symmetric fragmentation with five equal daughter particles

16 (Geometry 1) leads to the finest equilibrium contour plot but the contours are otherwise

17 unchanged. The granular disintegration geometries produced coarser results with the coarsest

18 armour from Geometry 4. We conclude that when fragmentation produces a number of

19 symmetric daughters the equilibrium grading of a hillslope is finest. Finally the slope of the

20 contours did not change for different fragmentation geometries.

5.2.6. Effect of initial conditions

22   The simulations in the sections above used the same grading for the initial surface and

23 the subsurface. To explore the initial conditions we changed the initial conditions. The

24 equilibrium grading contour plot generated using Ranger 2 surface grading and Ranger 1

25 bedrock gradings was identical to the equilibrium grading contour plot generated using

26 Ranger 1 surface and bedrock grading. Likewise the equilibrium grading contour plot

27 generated using Ranger 1 surface and Ranger 2 bedrock gradings was identical to the

28 equilibrium grading contour plot generated using Ranger 2 surface and bedrock for surface

29 and subsurface. However, the results were different for different subsurface gradings. These

30 results show that, as expected, there was no effect of the initial conditions on the equilibrium

31 grading. The influence of the initial grading is only felt during the dynamic phase of the

32 simulation before the armour reaches equilibrium.

5.3. Generalising beyond median grain size

The results above have focussed on d_{50} as a measure of soil grading. However, the model can provide any particle percentile or statistic of interest. Figure 10 shows area-slope results for d_{10} (i.e. 10% by mass is smaller than this diameter). It shows that the general trends observed in the d_{50} contour plots (Figure 5b2) are also evident in d_{10}. Though not shown, similar results were found for d_{90}. The slope of the contours is independent of diameter but as expected the d_{10} and d_{90} values are ranked $d_{10} < d_{50} < d_{90}$. We conclude that the area-slope-diameter relationship we have observed in our simulations is robust across the grading profile.

5.4. Influence of the depth dependent weathering functions

In this section we consider the three different depth dependent weathering functions (Figure 3, Equation 8 to 10) for the weathering rate in the subsurface soil layers. All the simulations in the previous sections used the exponential function (Equation 8). Figures 5 and 11 show that the contour plots for the armour for all weathering functions are very similar. However, as slope and area are increased the humped function produces a more rapidly coarsening armour. Overall the dynamic reversed exponential produces the coarsest armour. In this latter case after an initially high weathering rate at the surface, the weathering rate reduces rapidly as the soil-bedrock interface moves deeper into the soil profile. This slow near surface weathering increase the coarseness of the armour and dramatically reduces the erosion as well, preventing weathered fine particles from reaching the surface.

We also analysed the subsurface soil profile. Figure 12 shows the distribution d_{50} through the soil profile for a planar one-dimensional hillslope of length 32m, divided in to 8 nodes at 4 m intervals, and with 10% slope, and Ranger 1b bedrock. The bedrock layers are those layers near the base of the profile which have the maximum d_{50} (19mm). The exponential and humped functions produce similar soil profiles except the humped function produces a shallower soil and a coarser armour compared with the exponential. In contrast, the dynamic reversed exponential produces a markedly different soil profile. It produces very coarse armour, a soil thickness beyond the modelled 2000mm limit, and a more uniform soil grading through the profile. This latter result is because the weathering is greatest at the bedrock-soil interface so most of the soil grading change is focussed at the base of the profile and relatively less occurs within the profile.

1   A final question is whether the area-slope-grading relationship occurs only in the

2   armour or exists throughout the profile using the exponential weathering function. We

3   generated area-slope-d50 contours for four different depths within the profile (Figure 13).

4   The slope of the contours is the same for all depths and hence we believe that the area-slope-

5   grading log-log linear relationship is exhibited for the entire soil profile, with the only change

6   being the coarseness of the soil (which reflects the maturity of weathering of the soils) at any

7   particular depth.

8   **6. Discussion**

9   Here we have used a new and more general pedogenesis model, SSSPAM5D, to

10   analyse the equilibrium soil grading. Our results have generalised previous studies (Cohen et

11   al., 2009, 2010) that have found a log-log linear relationship between d_{50}, contributing area

12   and slope. Using a broader range of environmental conditions, we have found that log-log

13   linear relationship for grading is robust against changes in environment and underlying

14   geology and for hillslopes where the dominant processes are surface fluvial erosion and in-

15   profile weathering. The main factors influencing the quantitative form of the relationship are

16   the area and slope dependency of the erosion equation, and the relative rates of the

17   weathering and erosion processes. Coarsening of the downslope nodes was observed in all the

18   simulations.

19   Our parametric study has demonstrated the versatility of our model for studying the

20   influence of different process parameters and dynamics of evolution of hillslopes. Our d_{10} and

21   d_{90} contour plots show that the area-slope-diameter relationship is not only true for d_{50} but is

22   also true for other aspects of the particle size grading of the soil. This strengthens our

23   confidence in the generality of the area-slope-diameter relationship.   This relationship

24   provides us with a methodology to predict the characteristics of soil grading on a hillslope as

25   a function of geomorphology. It also allows us to interpolate between field measurements.

26   Furthermore, our parametric study showed how parameters of the armouring component

27   affect the area-slope-diameter relationship. Particularly interesting was that the ratio of the

28   erosion exponents (α_1/α_2) changes the slope of the contours. This observation also hints at the

29   importance of topographic and process characteristics in soil evolution and hillslope catena

30   and how these topographical units may be used for predictive soil mapping and inference of

31   erosion process.

1   Previous work (e.g. Willgoose, et al., 1991b; Tucker and Whipple, 2002) has shown

2   that topography is also a function of α_1/α_2 and this suggests a strong underlying process link

3   between the spatial distribution of topography and the spatial distribution of soil grading that

4   goes beyond the concept of soil catena. Soil catena says that systematic changes occur in soils

5   as a function of their position on the hillslope. Our results suggest that the same processes

6   that influence the equilibrium distribution of topography (e.g. the erosion process that

7   determines α_1/α_2) also influence the equilibrium distribution of soils. Thus while soil catena

8   presumes a causal link from topography, we postulate a causal link for both topography and

9   soils from erosion processes.

10   Using our model we were able to explore the soil profile characteristics and how the

11   soil profile will change depending on the weathering characteristics of the bedrock material.

12   Another important insight is that the area-slope-d_{50} relationship is present in all the subsurface

13   layers as well as the surface armour.

14   In this paper we have only considered erosion from overland fluid flow and physical

15   weathering mechanisms to predict the equilibrium soil distribution of hillslopes. There is a

16   need to explicitly incorporate chemical and biological weathering [*Green et al.*, 2006; *Lin*,

17   2011; *Riebe et al.*, 2004; *Roering et al.*, 2002; *Vanwalleghem et al.*, 2013]. Another important

18   aspect needed is accounting for deposition of sediments so that we can model alluvial soils.

19   An open question is how to incorporate a soils model like SSSPAM5D into a landform

20   evolution model such as SIBERIA [*Willgoose et al.*, 1991a]. If soils evolve rapidly then it

21   may be possible to use the equilibrium grading results from this paper as the soilscape model,

22   on the basis that the soil evolves fast enough to always be at, or near, equilibrium with the

23   evolving landform. If soils evolve slowly then it may be necessary to fully couple the soils

24   and landform evolution models. This is a subtle, and not fully resolved, question of relative

25   response times of the soils and the landforms [Willgoose et al., 2012].

26   **7. Conclusions**

27   The most important insight from this paper is that the area-slope-grading relationship

28   observed from a earlier generation soil profile pedogenesis model by previous authors (Cohen

29   et al., 2009, 2010) is general and robust across a range of climate and geologic conditions. In

30   spite of the wide range of parameters we used in our simulations, we always observed the

31   log-log linear area-slope-diameter relationship in our simulations although the soil coarseness

32   depended on the parameters used. In addition, contour plots of d_{10} and d_{90} indicated that the

1   area-slope-diameter relationship is valid throughout the soil grading range, not just for d_{50}. It

2   was also true for depths below the surface. The parametric study conducted on the area-slope-

3   diameter relationship demonstrated how this relationship would change with changes in the

4   pedogenic processes. We found that the ratio of the erosion exponents on discharge and

5   slope, α_1/α_2, changes the angle of the contours in the log-log contour plots (Figures 7). This

6   has application in the field of digital soil mapping where easily measurable topographical

7   properties can be used to predict the characteristics of soil properties. Importantly, the

8   contributing area and the slope data can be easily derived from a digital elevation model,

9   which can be produced using remote sensing and GIS techniques. Coupling SSSPAM5D with

10 a GIS system can potentially revolutionize the field of digital soil mapping by providing a

11 physical basis to existing empirical methods and potentially streamlining existing resource

12 intensive and time-consuming soil mapping techniques as, for example, in the current

13 initiatives in global digital soil mapping (Sanchez et al., 2009).

14   The simple physical processes currently implemented in SSSPAM5D also enables it

15 to model the evolution of hillslope soil grading. A subsequent paper will focus on the

16 dynamics of the soil profile evolution process. Although we used only armouring and

17 weathering as soil forming factors in this study, other processes such as chemical weathering

18 or biological influence on soil formation can also be included in our state-space matrix

19 modelling framework (e.g. Willgoose, "Models of Landscape and Soilscape Evolution", in

20 prep). With its high computational efficiency and ability to incorporate various processes in

21 to its modelling framework, SSSPAM5D has the potential to be a powerful tool for

22 understanding and modelling pedogenesis and its morphological implications.

24 **Acknowledgements**

25 This work was supported by Australian Research Council Discovery Grant DP110101216.

26 The SSSPAM5D model and the parameters used in this paper are available on request from

27 the authors.

1 **References**

2 Ahnert, F. (1977), Some comments on the quantitative formulation of geomorphological
3 processes in a theoretical model, *Earth Surface Processes*, *2*(2-3), 191-201,
4 doi:10.1002/esp.3290020211.

6 Behrens, T., and T. Scholten (2006), Digital soil mapping in Germany—a review, *Journal of*
7 *Plant Nutrition and Soil Science*, *169*(3), 434-443, doi:10.1002/jpln.200521962.

9 Benites, V. M., P. L. O. A. Machado, E. C. C. Fidalgo, M. R. Coelho, and B. E. Madari
10 (2007), Pedotransfer functions for estimating soil bulk density from existing soil survey
11 reports in Brazil, *Geoderma*, *139*(1–2), 90-97,
12 doi:http://dx.doi.org/10.1016/j.geoderma.2007.01.005.

14 Cohen, S., G. Willgoose, and G. Hancock (2009), The mARM spatially distributed soil
15 evolution model: A computationally efficient modeling framework and analysis of hillslope
16 soil surface organization, *J. Geophys. Res.-Earth Surf.*, *114*,
17 doi:F0300110.1029/2008jf001214.

19 Cohen, S., G. Willgoose, and G. Hancock (2010), The mARM3D spatially distributed soil
20 evolution model: Three-dimensional model framework and analysis of hillslope and landform
21 responses, *J. Geophys. Res.-Earth Surf.*, *115*, doi:F0401310.1029/2009jf001536.

23 Coulthard, T. J., G. R. Hancock, and J. B. C. Lowry (2012), Modelling soil erosion with a
24 downscaled landscape evolution model, *Earth Surf. Process. Landf.*, *37*(10), 1046-1055,
25 doi:10.1002/esp.3226.

27 Gessler, J. (1970), Self-stabilizing tendencies of alluvial channels, *Journal of the Waterways,*
28 *Harbors and Coastal Engineering Division*, *96*(2), 235-249.

30 Gomez, B. (1983), Temporal variations in bedload transport rates: The effect of progressive
31 bed armouring, *Earth Surf. Process. Landf.*, *8*(1), 41-54, doi:10.1002/esp.3290080105.

33 Green, E. G., W. E. Dietrich, and J. F. Banfield (2006), Quantification of chemical
34 weathering rates across an actively eroding hillslope, *Earth and Planetary Science Letters*,
35 *242*(1–2), 155-169, doi:http://dx.doi.org/10.1016/j.epsl.2005.11.039.

37 Hillel, D. (1982), *Introduction to soil physics*, Academic Press.

39 Humphreys, G. S., and M. T. Wilkinson (2007), The soil production function: A brief history
40 and its rediscovery, *Geoderma*, *139*(1–2), 73-78,
41 doi:http://dx.doi.org/10.1016/j.geoderma.2007.01.004.

43 Lin, H. (2011), Three Principles of Soil Change and Pedogenesis in Time and Space, *Soil Sci.*
44 *Soc. Am. J.*, *75*(6), 2049-2070, doi:10.2136/sssaj2011.0130.

46 Lisle, T., and M. Madej (1992), Spatial variation in armouring in a channel with high
47 sediment supply, *Dynamics of gravel-bed rivers*, 277-293.

2   Little, W. C., and P. G. Mayer (1976), Stability of channel beds by armoring, *Journal of the*
3   *Hydraulics Division-Asce*, *102*(11), 1647-1661.

5   McBratney, A. B., M. L. Mendonça Santos, and B. Minasny (2003), On digital soil mapping,
6   *Geoderma*, *117*(1–2), 3-52, doi:http://dx.doi.org/10.1016/S0016-7061(03)00223-4.

8   Minasny, B., and A. B. McBratney (2006), Mechanistic soil-landscape modelling as an
9   approach to developing pedogenetic classifications, *Geoderma*, *133*(1-2), 138-149,
10   doi:10.1016/j.geoderma.2006.03.042.

12   Ollier, C. (1984), *Weathering*, Longman Group.

14   Parker, G., and P. C. Klingeman (1982), On why gravel bed streams are paved, *Water*
15   *Resour. Res.*, *18*(5), 1409-1423, doi:10.1029/WR018i005p01409.

17   Riebe, C. S., J. W. Kirchner, and R. C. Finkel (2004), Erosional and climatic effects on long-
18   term chemical weathering rates in granitic landscapes spanning diverse climate regimes,
19   *Earth and Planetary Science Letters*, *224*(3–4), 547-562,
20   doi:http://dx.doi.org/10.1016/j.epsl.2004.05.019.

22   Roering, J. J., P. Almond, P. Tonkin, and J. McKean (2002), Soil transport driven by
23   biological processes over millennial time scales, *Geology*, *30*(12), 1115-1118.

25   Sanchez, P. A., et al. (2009), Digital soil map of the world, *Science*, *325*(5941), 680-681.

26   Scull, P., J. Franklin, O. Chadwick, and D. McArthur (2003), Predictive soil mapping: a
27   review, *Progress in Physical Geography*, *27*(2), 171-197.

29   Sharmeen, S., and G. R. Willgoose (2006), The interaction between armouring and particle
30   weathering for eroding landscapes, *Earth Surf. Process. Landf.*, *31*(10), 1195-1210,
31   doi:10.1002/esp.1397.

33   Sharmeen, S., and G. R. Willgoose (2007), A one-dimensional model for simulating
34   armouring and erosion on hillslopes: 2. Long term erosion and armouring predictions for two
35   contrasting mine spoils, *Earth Surf. Process. Landf.*, *32*(10), 1437-1453,
36   doi:10.1002/esp.1482.

38   Singh, V., and D. Woolhiser (2002), Mathematical Modeling of Watershed Hydrology,
39   *Journal of Hydrologic Engineering*, *7*(4), 270-292, doi:doi:10.1061/(ASCE)1084-
40   0699(2002)7:4(270).

42   Strahler, A. H., and A. N. Strahler (2006), *Introducing physical geography*, J. Wiley.
43   Thornbury, W. D. (1969), *Principles of geomorphology*, Wiley New York.

44

45   Tucker, G. E., and K. X. Whipple (2002), Topographic outcomes predicted by stream erosion
46   models: Sensitivity analysis and intermodel comparison, *Journal of Geophysical Research-*
47   *Solid Earth*, *107*(B9), art. no.-2179.

48

1   Vanwalleghem, T., U. Stockmann, B. Minasny, and A. B. McBratney (2013), A quantitative
2   model for integrating landscape evolution and soil formation, *Journal of Geophysical*
3   *Research: Earth Surface*, *118*(2), 331-347, doi:10.1029/2011JF002296.
4
5   Wells, T., P. Binning, G. Willgoose, and G. Hancock (2006), Laboratory simulation of the
6   salt weathering of schist: I. Weathering of schist blocks in a seasonally wet tropical
7   environment, *Earth Surf. Process. Landf.*, *31*(3), 339-354, doi:10.1002/esp.1248.
8
9   Wells, T., G. R. Willgoose, and G. R. Hancock (2008), Modeling weathering pathways and
10 processes of the fragmentation of salt weathered quartz-chlorite schist, *J. Geophys. Res.-*
11 *Earth Surf.*, *113*(F1), doi:F0101410.1029/2006jf000714.

13 Willgoose, G., R. L. Bras, and I. Rodriguez-Iturbe (1991a), A coupled channel network
14 growth and hillslope evolution model: 1. Theory, *Water Resour. Res.*, *27*(7), 1671-1684,
15 doi:10.1029/91wr00935.
16
17 Willgoose, G., R. L. Bras, and I. Rodriguez-Iturbe (1991b), A physical explanation of an
18 observed link area-slope relationship, *Water Resour. Res.*, *27*(7), 1697-1702,
19 doi:10.1029/91wr00937.
20
21 Willgoose, G., and S. Riley (1998), The long-term stability of engineered landforms of the
22 Ranger Uranium Mine, Northern Territory, Australia: Application of a catchment evolution
23 model, *Earth Surf. Process. Landf.*, *23*(3), 237-259, doi:10.1002/(sici)1096-
24 9837(199803)23:3<237::aid-esp846>3.0.co;2-x.
25
26 Willgoose, G. R., S. Cohen, G. R. Hancock, E. U. Hobley, and P. M. Saco (2012), The co-
27 evolution and spatial organisation of soils, landforms, vegetation, and hydrology, in
28 *American Geophysical Union Fall Meeting*, EP42D-01, San Francisco.

29 Yokoyama, T., and Y. Matsukura (2006), Field and laboratory experiments on weathering
30 rates of granodiorite: Separation of chemical and physical processes, *Geology*, *34*(10), 809-
31 812.

1 **Figures**

2   **Figure 1**
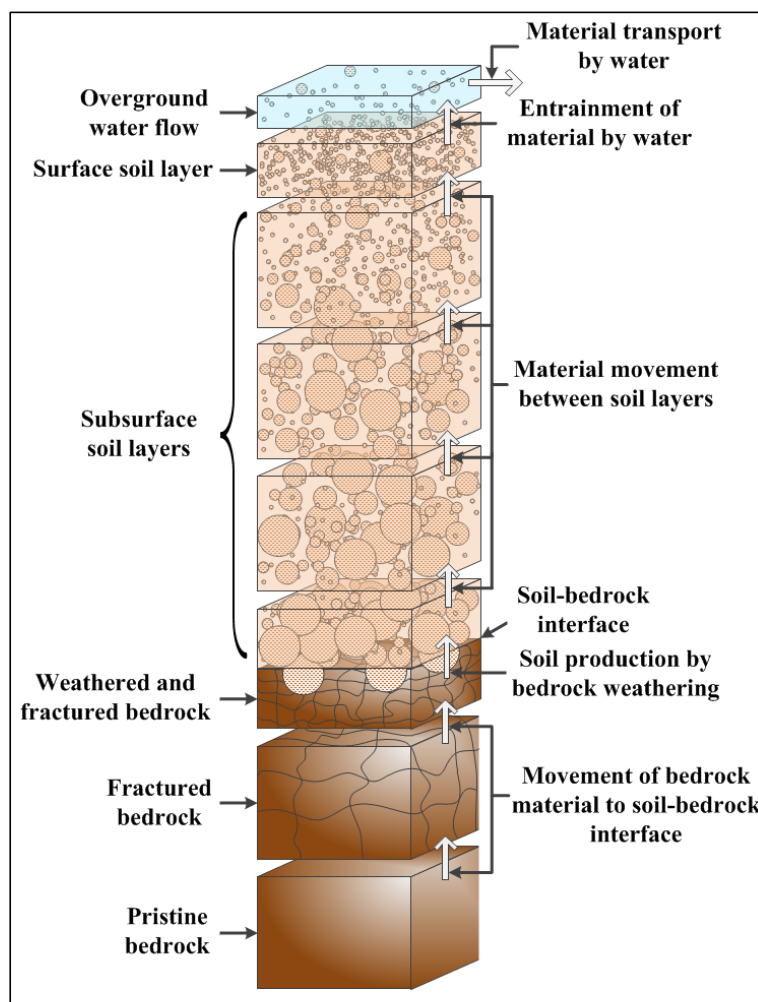
4   **Figure 1:** Schematic diagram of the SSSPAM5D model (from Cohen et al., 2010).
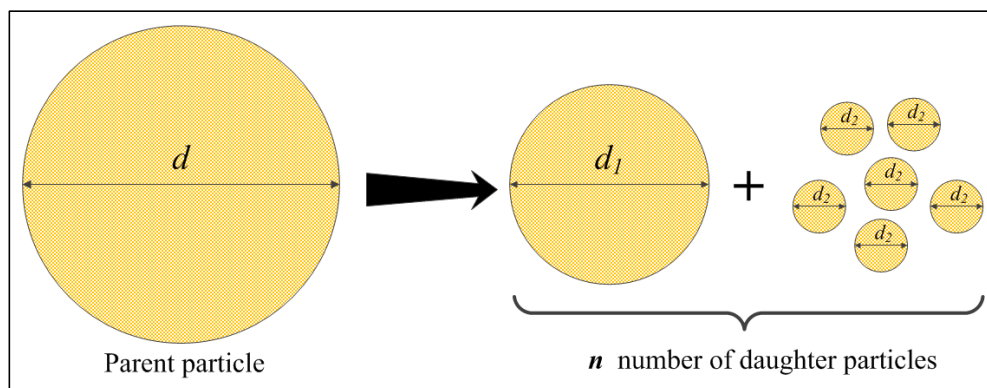
1   **Figure 2**

3   **Figure 2:** The fragmentation geometry used in SSSPAM5D (after Wells, et al., 2008).
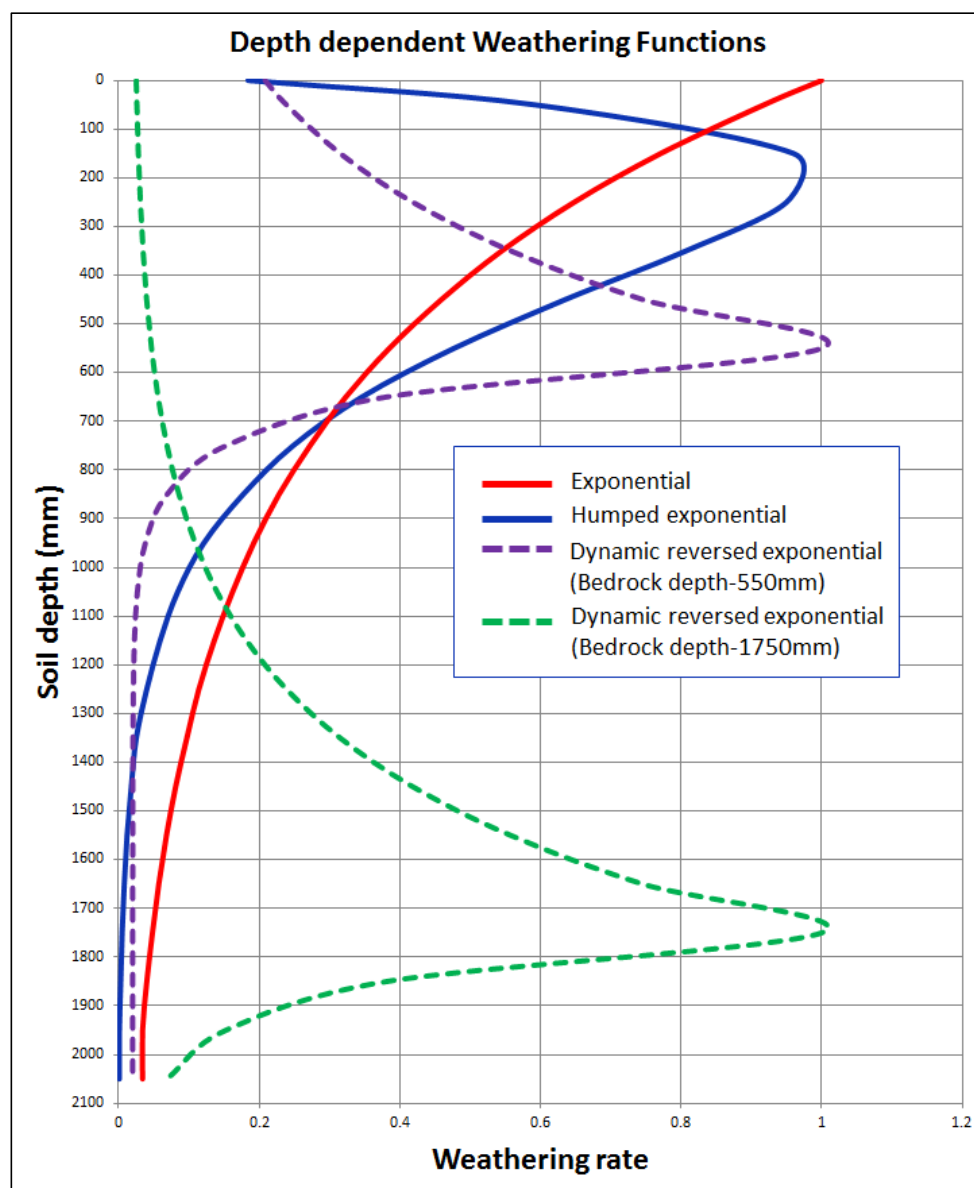
1   **Figure 3**

3   **Figure 3:** Graphical representation of all the depth dependent weathering functions used in
4   SSSPAM5D

Earth **Surface**
Dynamics
Discussions
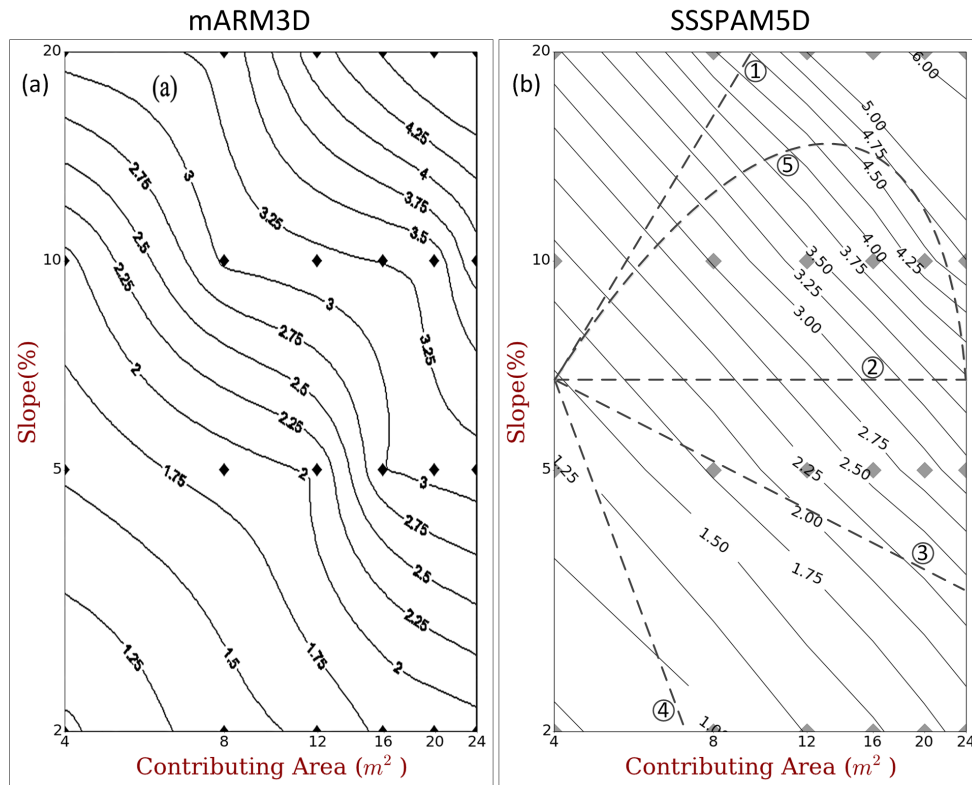
1   **Figure 4**

Figure 4: Log-log Area-Slope-d_{50} contour plots generated using Ranger1 data set. (a) mARM3D [*Cohen et al.*, 2010], (b) SSSPAM5D. The dotted lines in (b) are hypothetical hillslope profiles showing how the contour figure can be used to generate soil properties down a hillslope. See the text for more detail.
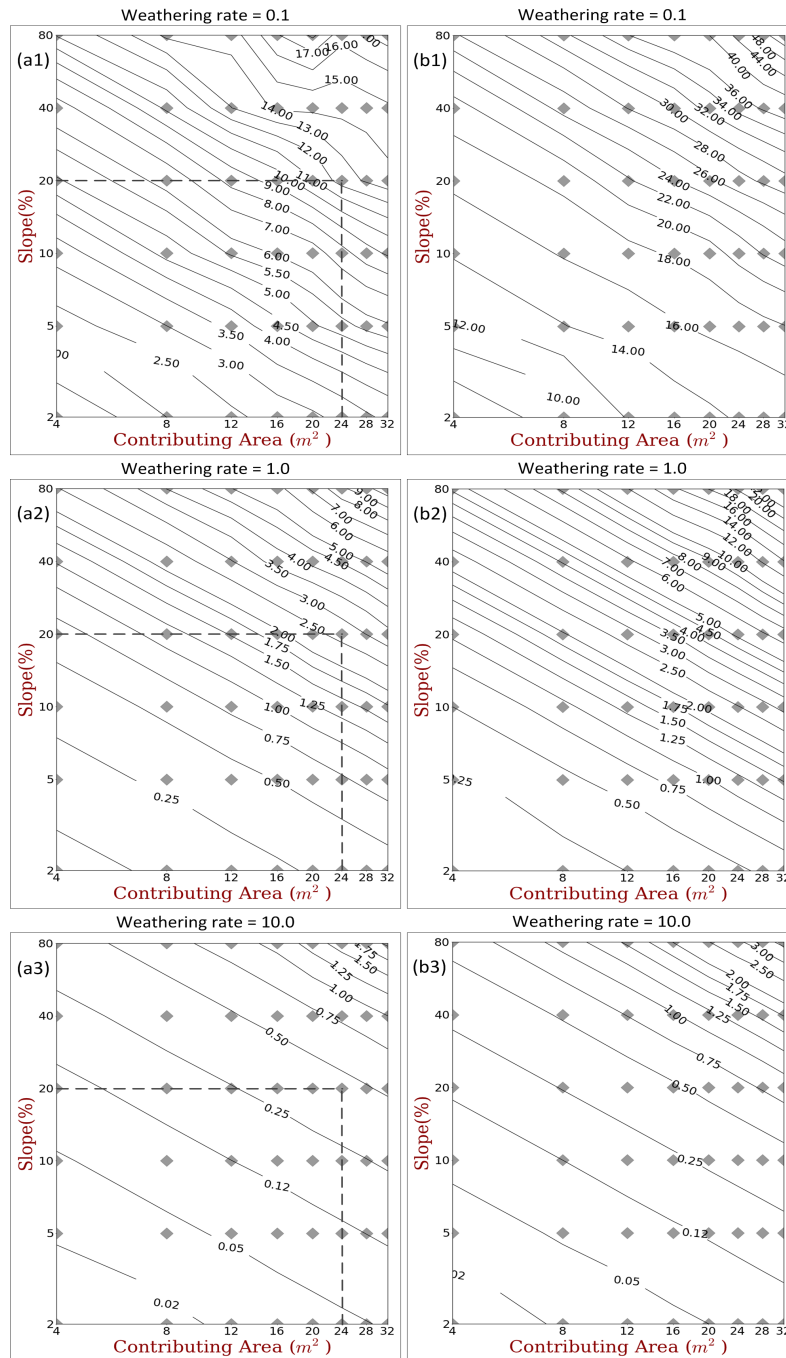
1   **Figure 5**

1 **Figure 5:** Equilibrium contour plots of d_{50} values (interpolated from 48 data values, the
2 diamonds) simulated by SSSPAM5D for different surface and subsurface grading data and
3 different weathering rates (Top to Bottom: 0.1, 1.0, 10.0). (Left Column) Ranger1 grading,
4 (Right Column) Ranger2 grading.
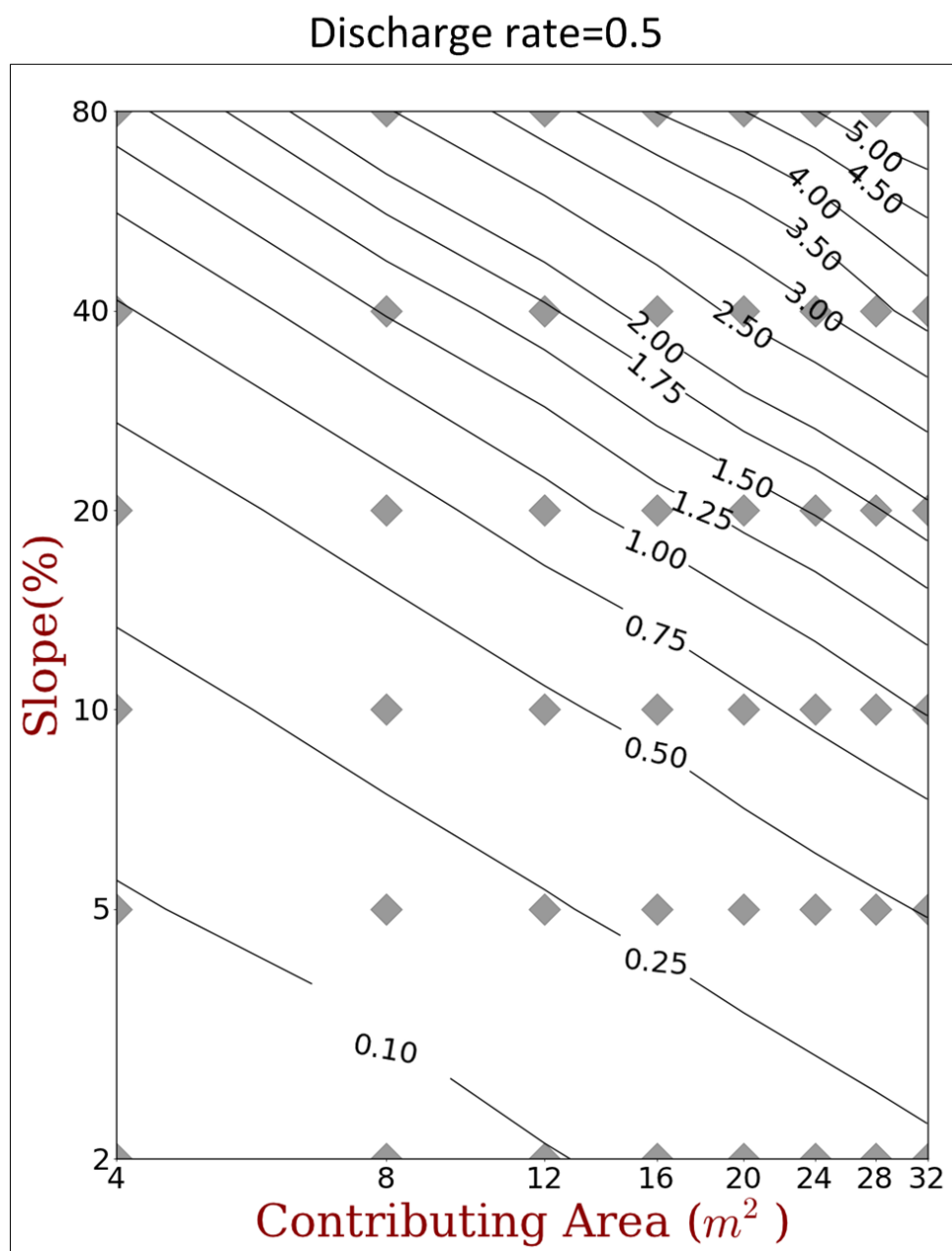
1   **Figure 6**

3   **Figure 6:** Equilibrium contour plots of d_{50} generated using Ranger1 data with identical model
4   parameters as Figure 5(a2) except changing the runoff rate, half the nominal rate
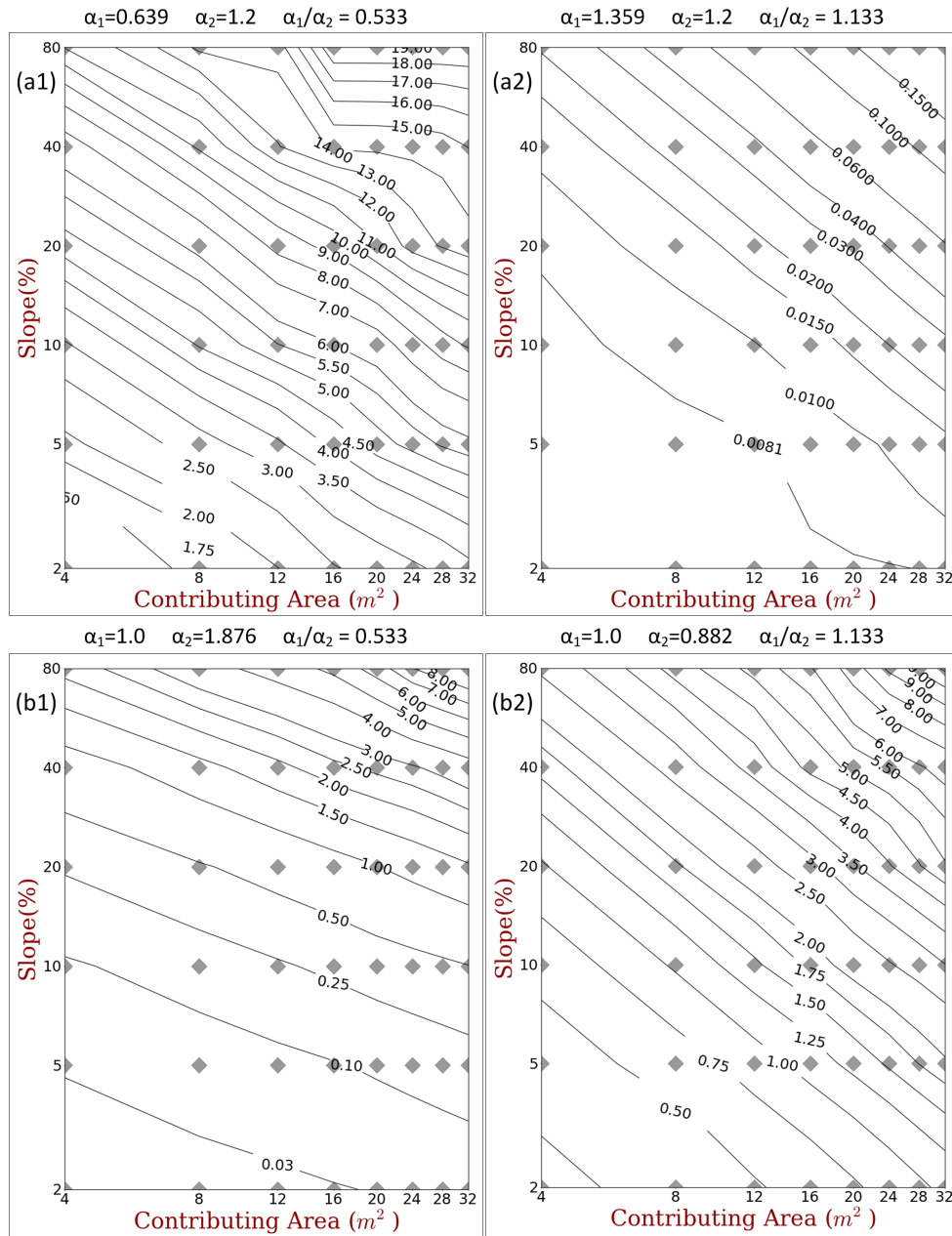
Figure 7: Equilibrium contour plots of d_{50} generated using Ranger 1 data with identical
model parameters as Figure 5(a2) (i.e. α_1=1.0, α_2=1.2, α_1/α_2=0.833) except changing α_1 and α_2
values generated using (a1, b1) different α_1 and constant α_2 values, (a2, b2) different α_2 and
constant α_1 values.
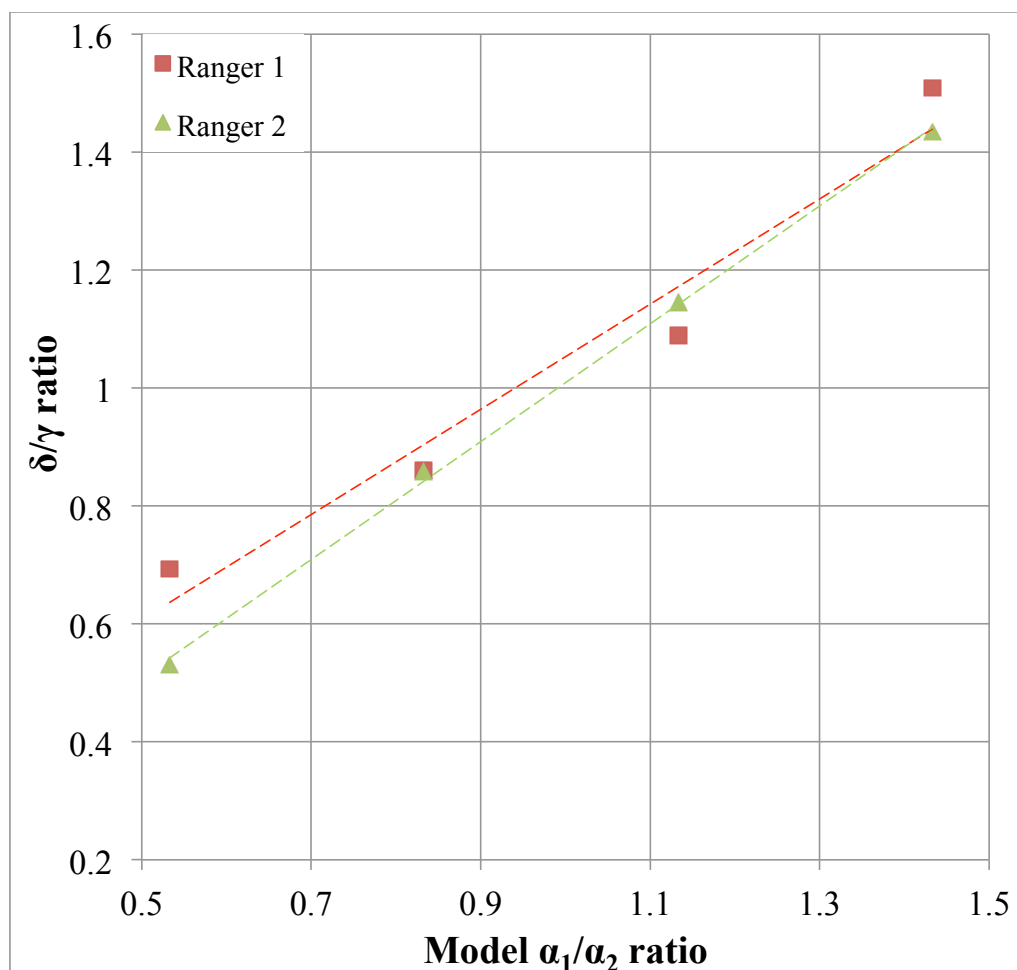
2   **Figure 8**

4   **Figure 8:** Correlation between the model α_1/α_2 and δ/γ
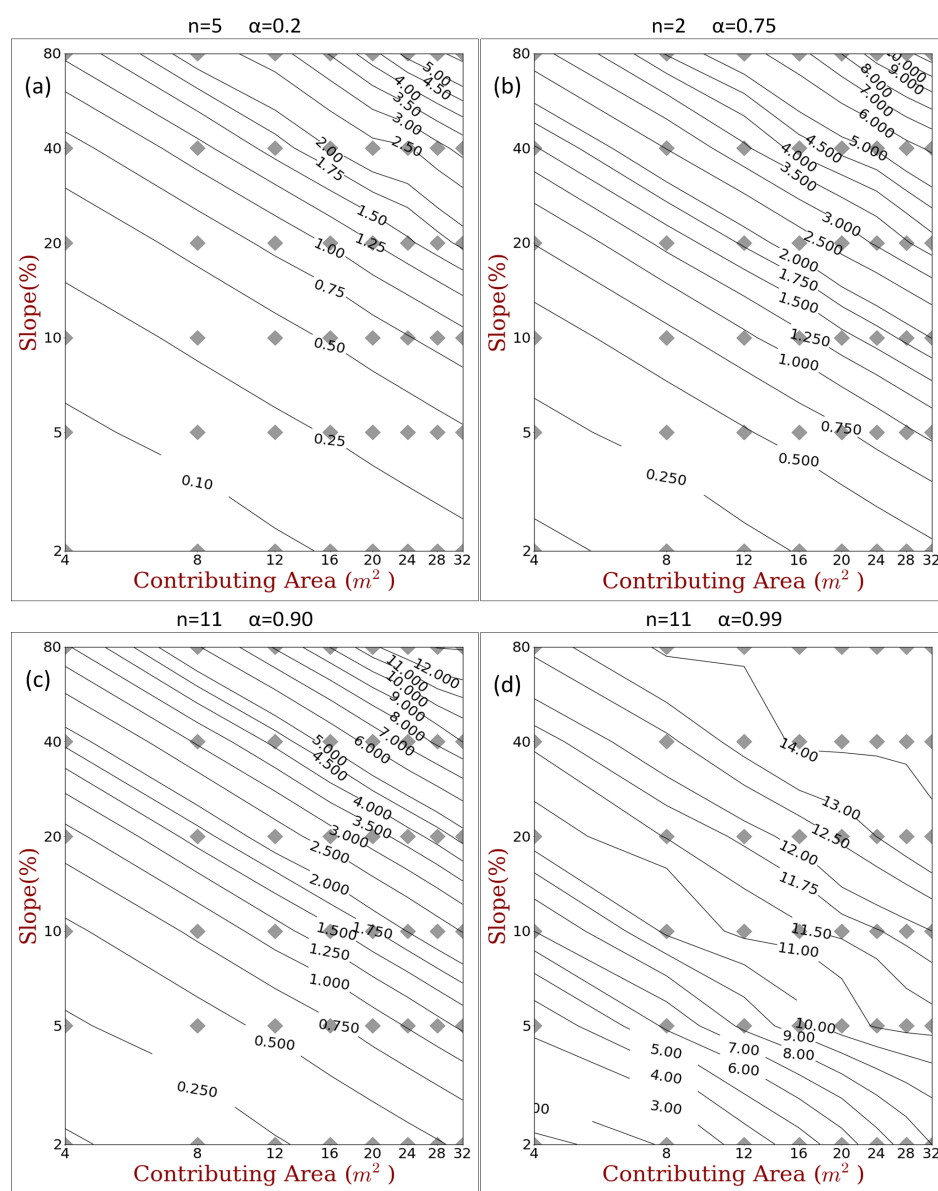
1   **Figure 9**

3   **Figure 9:** Equilibrium contour plots of d_{50} generated using Ranger1 grading data with
4   identical model parameters as Figure 5(a2) (i.e. n=2, α=0.5; symmetric fragmentation with 2
5   daughter particles) except changing the weathering geometry, n-number of daughter particles
6   and α - material fraction retained by largest daughter particle (a) symmetric fragmentation
7   with n=5 and α=0.2 (b) asymmetric fragmentation with n=2 and α=0.75 (c) granular
8   disintegration with n=11 and α=0.9, (d) granular disintegration with n=11 and α=0.99.
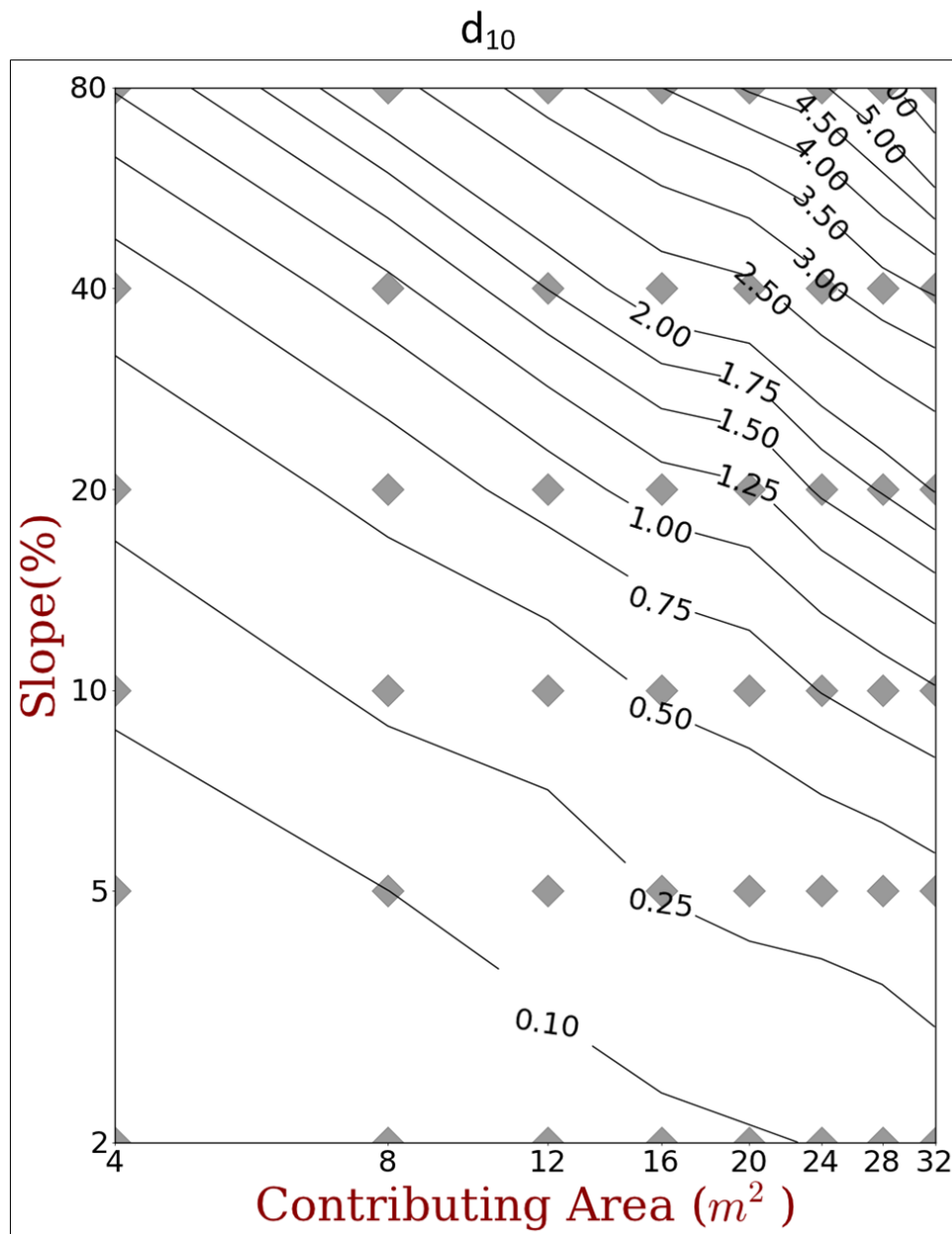
Figure 10

4   **Figure 10:** Equilibrium contour plots of d_{10} generated using Ranger1 grading data with

5   identical model parameters as Figure 5(a2) (where the d_{50} results are presented).
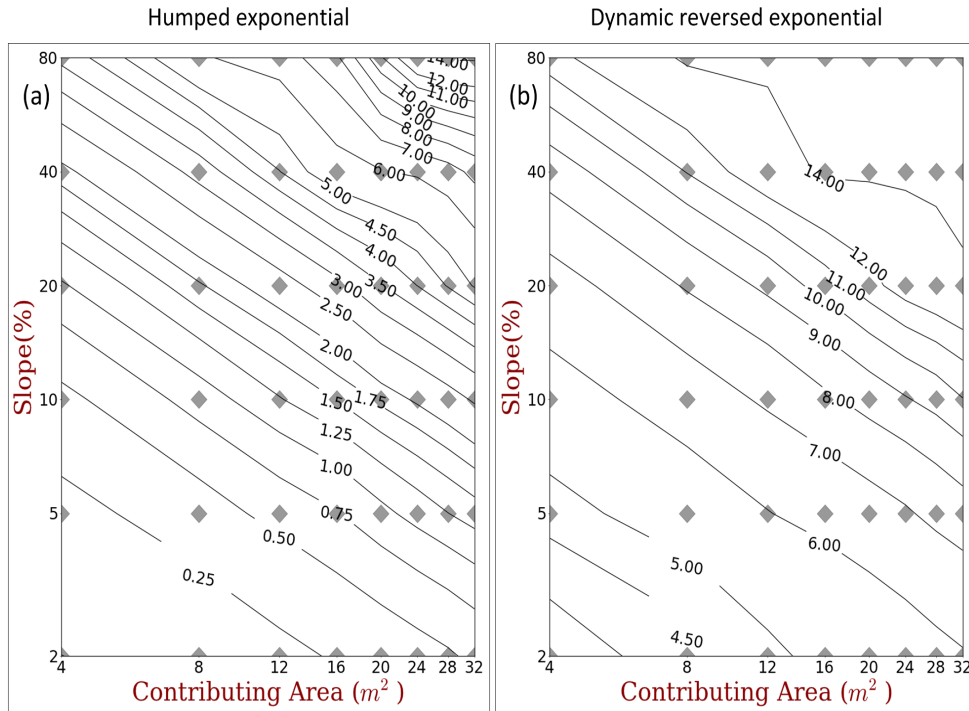
2   **Figure 11**

4   **Figure 11:** Equilibrium contour plots of d_{50} generated using Ranger 1 grading data with

5   identical model parameters as Figure 5(a2) except changing the depth dependent weathering

6   function to (a) Humped, (b) Dynamic reversed exponential.

1   **Figure 12**
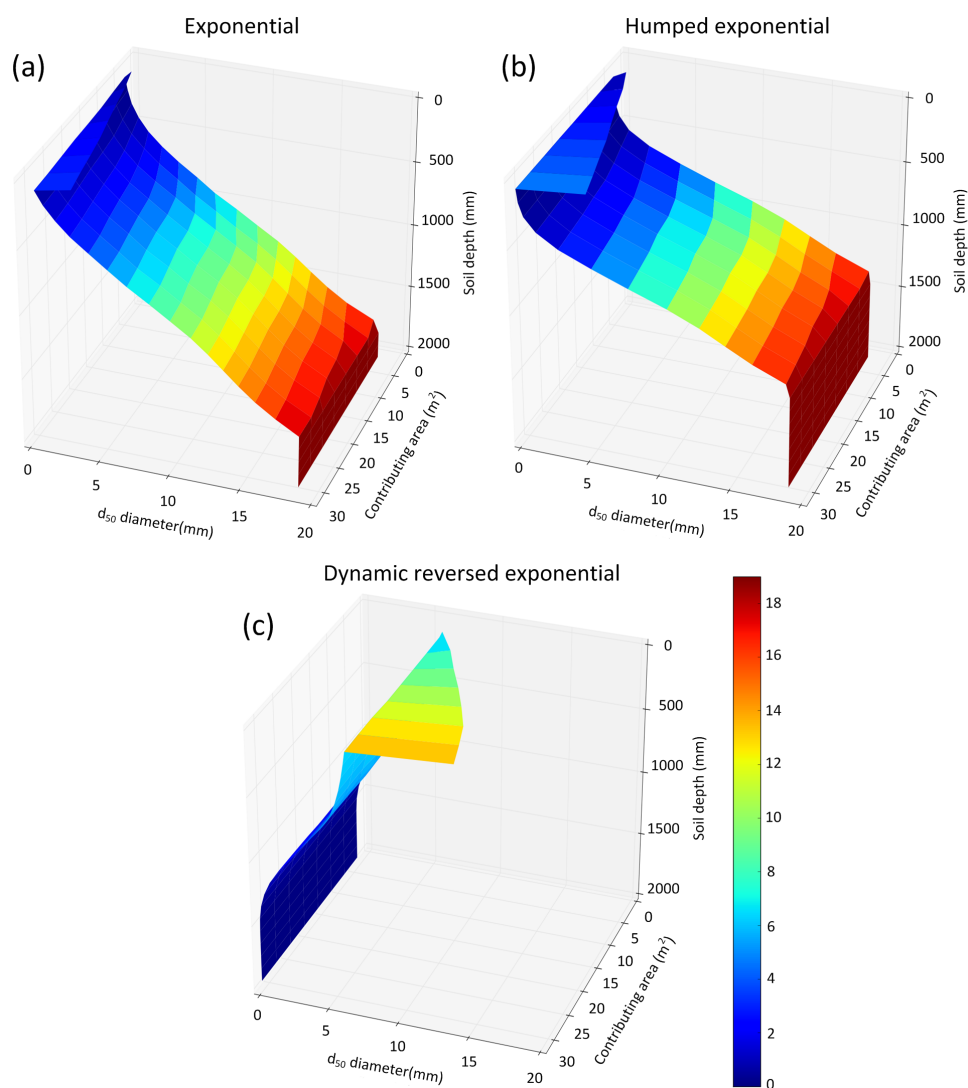
5   **Figure 12:** Equilibrium soil profile d_{50} generated using the Ranger1 grading with a one-
6   dimensional hillslope with 10% slope and 32m length using (a) Exponential, (b) Humped, (c)
7   Dynamic reversed exponential weathering functions.
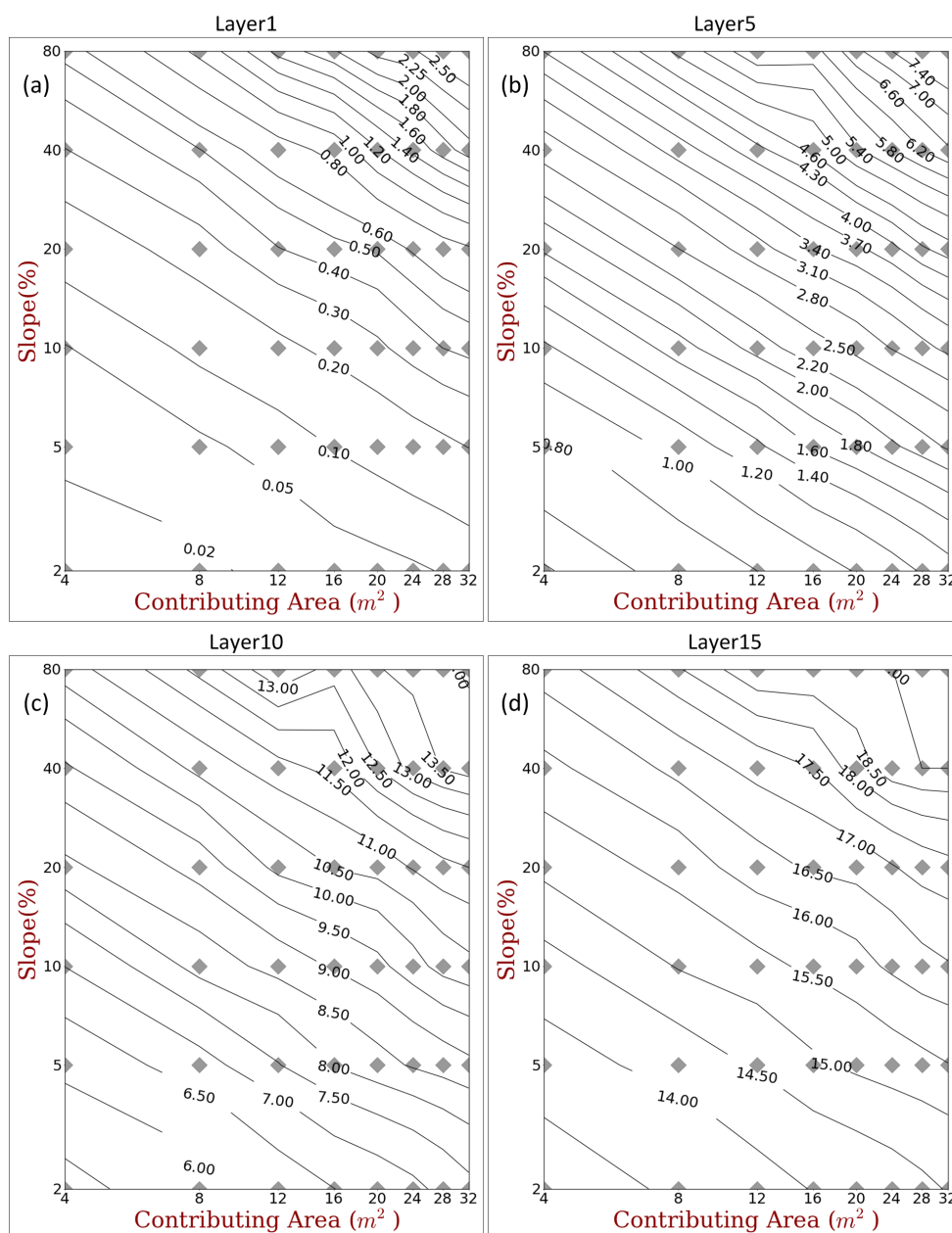
1 **Figure 13**

3 **Figure 13:** Equilibrium contour plots of d_{50} generated using Ranger 1 grading data with

4 identical model parameters as Figure 5(a2) for different subsurface soil layers (a) layer 1

5 (100mm depth), (b) layer 5 (500mm depth), (c) layer 10 (1000mm depth), (b) layer 15

6 (1500mm depth)

1 **Tables**

2 **Table 1.** Size distribution of soil gradings used for SSSPAM4D simulations

Grading Range (mm)			Ranger 1	Ranger 1 bedrock	Ranger 2	Ranger 2 bedrock
0	-	0.063	1.40 %	0.0%	8.75 %	0.0%
0.063	-	0.111	2.25 %	0.0%	2.19 %	0.0%
0.111	-	0.125	0.75 %	0.0%	1.46 %	0.0%
0.125	-	0.187	1.15 %	0.0%	1.72 %	0.0%
0.187	-	0.25	1.15 %	0.0%	0.86 %	0.0%
0.25	-	0.5	10.20 %	0.0%	0.86 %	0.0%
0.5	-	1	9.60 %	0.0%	0.86 %	0.0%
1	-	2	12.50 %	0.0%	0.86 %	0.0%
2	-	4	16.40 %	0.0%	5.70 %	0.0%
4	-	9.5	20.00 %	0.0%	6.35 %	0.0%
9.5	-	19	24.60 %	100.0%	7.65 %	0.0%
19	-	40	0.00 %	0.0%	8.70 %	0.0%
40	-	95	0.00 %	0.0%	12.85 %	0.0%
95	-	200	0.00 %	0.0%	41.20 %	100.0%

13 **Table 2.** Parameters used in the simulations generate Figure 5(a2)

Equation No	Parameter	Value
3	α_1	1.0
	α_2	1.2
	β	1.0
	e	0.025
5,6,7	α	0.5
	n	2.0
8	β'	1.0
	δ_1	1.738
9	P_0	0.25
	P_a	0.02
	δ_2	4.0
	δ_3	6.0
	M	0.04
10	λ	0.98
	δ_4	3
	δ_5	10

2   **Table 3.** Parameters of the d_{50}-Area-Slope relationship calculated from regression analysis

3   for different data sets and different model α_1/α_2 ratios.

α_1	α_2	α_1/α_2	δ	γ	δ/γ
Ranger grading data set 1					
0.800	1.500	**0.533**	0.620	0.894	**0.694**
1.000	1.200	**0.833**	0.805	0.936	**0.859**
1.020	0.900	**1.133**	0.798	0.733	**1.088**
1.200	0.837	**1.433**	0.725	0.480	**1.509**
Ranger grading dataset 2					
0.800	1.500	**0.533**	0.701	1.322	**0.530**
1.000	1.200	**0.833**	0.437	0.509	**0.859**
1.020	0.900	**1.133**	0.909	0.794	**1.145**
1.200	0.837	**1.433**	0.843	0.588	**1.434**